Materials Science in Semiconductor Processing 179 (2024) 108480

Contents lists available at ScienceDirect

Materials Science in Semiconductor Processing

journal homepage: www.elsevier.com/locate/mssp

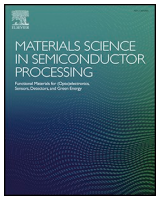

Thermal dependence of the current in TiN/Ti/HfO_2/W memristors at different intermediate conduction states

F. Jiménez-Molinos [a,*], G. Vinuesa [b], H. García [b], S. Dueñas [b], H. Castán [b], M.B. González [c], F. Campabadal [c], J.B. Roldán [a]

[a] Departamento de Electrónica y Tecnología de Computadores, Universidad de Granada, Facultad de Ciencias, Avd. Fuentenueva s/n, 18071, Granada, Spain
[b] Departamento de Electrónica, Universidad de Valladolid, Paseo de Belén 15, 47011, Valladolid, Spain
[c] Institut de Microelectrònica de Barcelona, IMB-CNM (CSIC), Carrer dels Til·lers s/n, Campus UAB, 08193, Bellaterra, Spain

A B S T R A C T

The dependence of the current in TiN/Ti/HfO_2/W devices on the temperature is investigated in the range from 78 K to 340 K. Resistive switching cycles at 78 K are conducted to explore the thermal dependence in filament configurations with different intermediate resistance states. The less conductive states show an increase of the current as the temperature rises, while the fully formed filament displays a metallic-like behavior. A comprehensive model, based on the Stanford Model including a series resistance, is proposed and successfully validated by experimental data. The interplay between the ohmic and non-linear components in the model for different filament states is analyzed, emphasizing the dominance of the non-linear component (and its corresponding thermal dependence) in partially formed filaments and the prevalence of the ohmic component in the fully formed filament, which shows a decreasing current as the temperature rises. A complete compact model for simulation of circuits including the thermal dependence of these devices is developed.

1. Introduction

Memristors have become key components in the cutting-edge advancements in the fields of non-volatile memories [1,2], hardware implementations of artificial intelligence systems [3–5] and cryptographic circuits [6]. Redox-based memristive devices, or Resistive Random-Access Memories (RRAMs), are two-terminal devices capable of altering their resistance through the application of appropriate voltage or current signals [7,8], in a non-volatile way. That is, the devices maintain their programmed resistance if the external excitation is removed. Usually, a forming process is required for creating a conductive path or filament through a pristine dielectric, whose nature strongly depends on the stack materials [9]. After that, RRAMs can transition between two distinct conduction states under the application of the programming signals: the low resistance state (LRS) and the high resistance state (HRS), although controllable intermediate states are also possible [10–12]. The processes that drive the filament to the (HRS) are called reset, while the filament undergoes reconstruction in the set processes. A resistive switching (RS) cycle comprises set-reset processes. Because of the inherent stochastic nature of the switching mechanisms involved, the reconstructed conductive filaments (CFs) differ from the previous ones, leading to cycle-to-cycle variability [13].

Various insulators in metal-insulator-metal (MIM) stacks exhibit resistive switching (RS), with two main types of RRAMs: valence change memories (VCM) and conductive bridge RRAMs. The present work focuses on TiN/Ti/HfO_2/W devices, belonging to the VCM category. In the studied memristors, the CFs are formed by regions with a high density of oxygen vacancies [14–16]. HfO_2-based devices, among several metal oxides demonstrating RS, stand out for their performance and compatibility with CMOS technology, although RS has been also demonstrated in HfO_2 nanocrystals [17]. Numerous studies on HfO_2 memristors with different electrode materials have been published. Typically, the devices are characterized using I–V plots of RS cycles, obtained under voltage ramp operation at room temperature. However, temperature influences both the RS and the charge transport mechanisms [15,18]. Therefore, a study of the temperature dependence is also necessary for a complete device characterization. This work will be focused on the thermal dependence of the current. Therefore, in order to isolate it from other effects (influence of the temperature on the formation/disruption of the CF and variability), the CF is maintained invariable during the temperature sweep (with this purpose the I–V characterization is limited to low voltages, below the thresholds that lead to set and reset processes, and there is no RS cycling). In a previous work [19], we presented a study that aimed to characterize and model the thermal dependence of the current in the LRS of TiN/Ti/HfO_2/Pt devices within a temperature range of 90 K–350 K, avoiding cycling to maintain a constant CF shape.

* Corresponding author.
E-mail address: jmolinos@ugr.es (F. Jiménez-Molinos).

https://doi.org/10.1016/j.mssp.2024.108480
Received 8 March 2024; Received in revised form 25 April 2024; Accepted 27 April 2024

In the present work, that model is generalized for intermediate states between the HRS and the LRS in devices based on the TiN/Ti/HfO_2/W stack, in a coherent way that maintains the core characteristics of the previous model.

The thermal dependence of the current in HfO_2 based RS devices has also been previously studied in different temperature ranges. For example, a weak thermal dependence in the LRS of TiN/HfO_2/Hf/TiN devices was observed for temperatures between 298 K and 468 K [20], while a higher influence was evidenced in TiN/HfO_2/TiN devices for a similar temperature range [21]. In a wider temperature interval (40K–350 K), significant current variation in Pt/Al_2O_3/HfO_x/Er/Pt devices was also measured; in this case, charge transport was attributed to inelastic trap-assisted tunneling [22]. Other works explore RS behavior at very low temperatures (4 K) in Pt/HfO_x/TiN memristors [23] and the effects of cycling on thermal dependence in TiN/HfO_2/Ti/TiN devices [24]. The current thermal dependence in the HRS and LRS of TaN/HfO_x/Ni memristors has also been studied [25], showing a weak thermal dependence of the LRS current, that disappears at lower temperatures (below 30 K). Finally, in a recent work [26], the current in the HRS and LRS of Au/Ti/HfO_x-Au devices is measured for 303 K and 453 K, showing an increase of the current as the temperature rises at low voltages. This variety of dependences justifies further studies to shed light on this issue, we do so here.

In particular, we empirically analyze and develop a model for the current-temperature dependence across a broad temperature range (78 K–340 K) in the LRS and in intermediate conduction states, reached after partial set processes. Through experiments conducted on TiN/Ti/HfO_2/W devices, the current is measured at low applied voltages, lower than the average set voltage. Therefore, under these operation conditions, the CFs are assumed not to change and all the variations in the device resistance can be attributed solely to thermal effects on the charge conduction mechanisms. These thermal dependences are integrated into a conduction model to provide an accurate portrayal of thermal effects.

As previously mentioned, memristors are promising components for the realization of neuromorphic circuits due to the memristor ability to mimic synaptic plasticity. In particular, the hardware implementation of neuronal networks (NNs) using memristors for simultaneously storing and processing the NN weights (in-memory computing) [3–5] can help to overcome the memory access bottleneck in the traditional software execution of deep NNs by von Neumann computers [27,28]. For the development of such circuits, and others based on memristors, it is essential to possess accurate models for their circuital simulation. Furthermore, as the working temperature could vary in a wide range, it is crucial to include the thermal dependencies in such models. In this context, we have developed this study and a modelling approach, which allows the simulation of circuits based on the studied memristors in SPICE simulators such as LTspice for a wide temperature range.

The paper is organized as follows: in section II, we introduce the device fabrication and measurement details. The experimental data are given in section III, while the modeling developments are tackled in section IV; finally, the main conclusions are summed-up in section V.

2. Experimental set-up

In order to carry out this study, resistive switching TiN/Ti/HfO_2/W memory devices were fabricated as follows. First, a 20 nm-thick Ti adherence layer was deposited on a Si-n^{++} wafer, followed by the deposition of the bottom electrode, that consists of a 50 nm-thick W layer.

Then, a 100 nm SiO_2 layer was grown by plasma-enhanced chemical vapor deposition (PECVD) using silane (SiH_4) as the precursor, which was then patterned by photolithography and dry etching to define the active area of the MIM devices. Next, the 10 nm HfO_2 insulator film was deposited by atomic layer deposition (ALD) at 225 °C using TDMAH and H_2O as precursors, and using N_2 as the carrier and purge gas. The top electrode, consisting of a 200 nm-thick TiN layer on a 10 nm-thick Ti layer, was grown by magnetron sputtering (as well as the bottom electrode) and patterned by a lift-off process. Finally, a 500 nm Al layer was deposited by magnetron sputtering on the back of the wafer for electrically contacting the W bottom electrode through the Si-n^{++} substrate. The studied TiN/Ti/HfO_2/W devices are square-shaped cells with an area of 40 × 40 μm^2. A cross-section of the devices can be seen in Fig. 1 (where a thin non-stoichiometric Ti oxide layer could be formed at the Ti/dielectric interface).

The electrical measurements were carried out using a Hewlett-Packard Semiconductor Parameter Analyzer 4155B. The voltage bias was always applied to the top electrode, while the bottom electrode remained grounded. The electrical characterization was performed in a wide temperature range, from 78 to 340 K in an Oxford Instruments Cryostat DM1710 using liquid nitrogen. The temperature was monitored by an Oxford Instruments Temperature Controller ITC 503 and the equipment was connected to a computer via GPIB interface and controlled using Agilent VEE software. A schematic of the experimental set-up can be seen in Fig. 2.

After performing the electroforming process (at 3.5 V with a current compliance of 10 μA) and before carrying out the temperature sweep, we first obtained the bipolar resistive switching I–V cycles at room temperature, which ranged from −1.3 V to +0.9 V. We then cooled the sample to 78 K, where we make a partial set, that is, from the HRS, we make an unfinished positive voltage sweep that should only partially form the conductive filament, leaving the device in an intermediate resistance state. Next, the temperature is increased, performing low voltage sweeps in the [−0.15 V, 0.15 V] range to not disrupt the intermediate state previously obtained (such low voltages are much lower than the switching voltages and should not provoke any change in the devices' resistance state). We perform this sweep at 78 K, 80 K and then every 10 K until a temperature of 340 K is reached, stabilizing every temperature at which electrical measurements are made. We repeated this measurement routine for different partial sets in order to obtain several intermediate states and observe the thermal dependencies of these conductive states. It must be noted that, after we achieved 340 K, we then measured several complete I–V resistive switching cycles at room temperature and at 78 K, in order to ensure that the complete RS cycle was still the same and the sample was not degrading. The routine was made as exposed for partial sets made at 0.45 V, 0.55 V, 0.65 V, 0.75 V, and lastly, for the complete set process at 0.9 V (although for this last case, there was no danger of accidently changing the state so the sweep is much larger ([−0.7 V, 0.7 V]). This was made to ensure that we obtained different resistance states, and thus, different partially formed filaments. As the set sweep reached higher voltage values, a higher conductance state was obtained, meaning that the filament was each time more formed than the previous, which allowed us to analyze how the temperature affects the different states and conductive filament

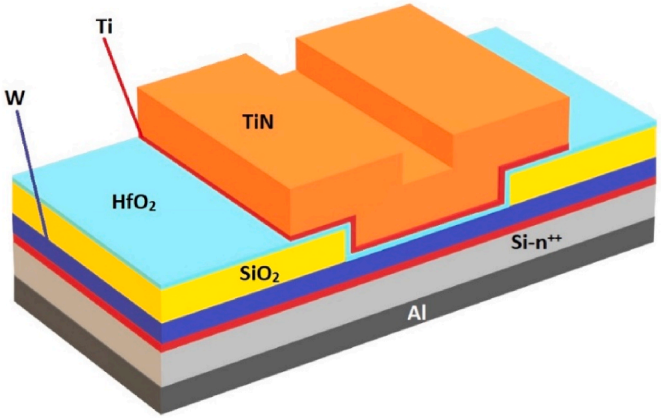

Fig. 1. Cross-section of the metal-insulator-metal TiN/Ti/HfO_2/W devices.

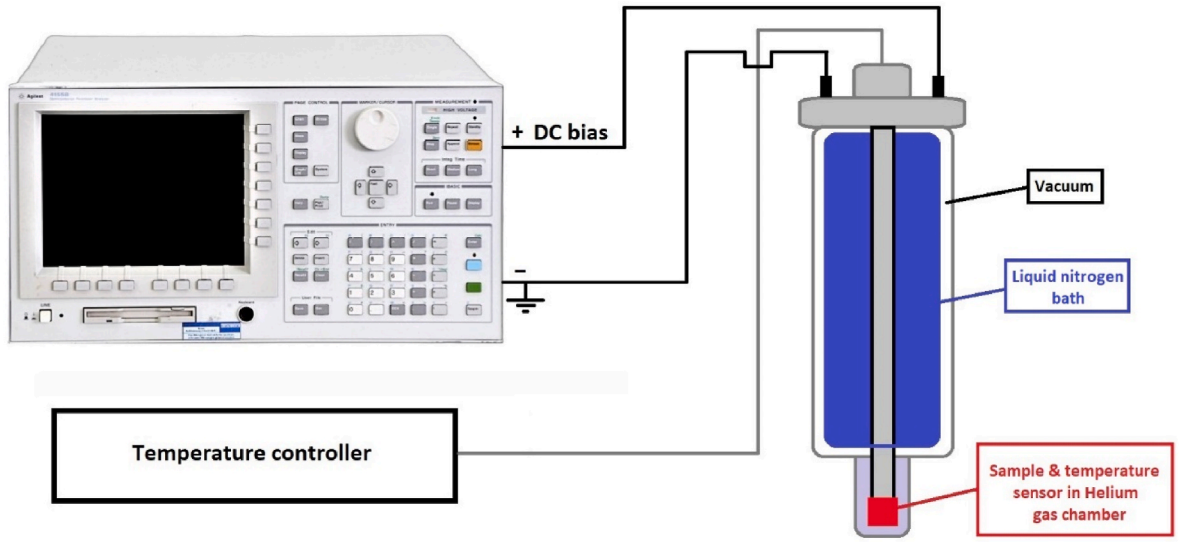

Fig. 2. Experimental set-up used for the thermoelectrical characterization of the devices.

configuration, and see how this dependency changes as the filament is more or less formed. The measuring process is further detailed on the flowchart of Fig. 3.

3. Experimental results

In addition to the current measurement in fixed intermediate conduction states, which will be shown below, RS cycles at different temperatures were performed (see Fig. 4a). As expected, the external temperature has an impact on the set and reset voltages. Fig. 4b and c

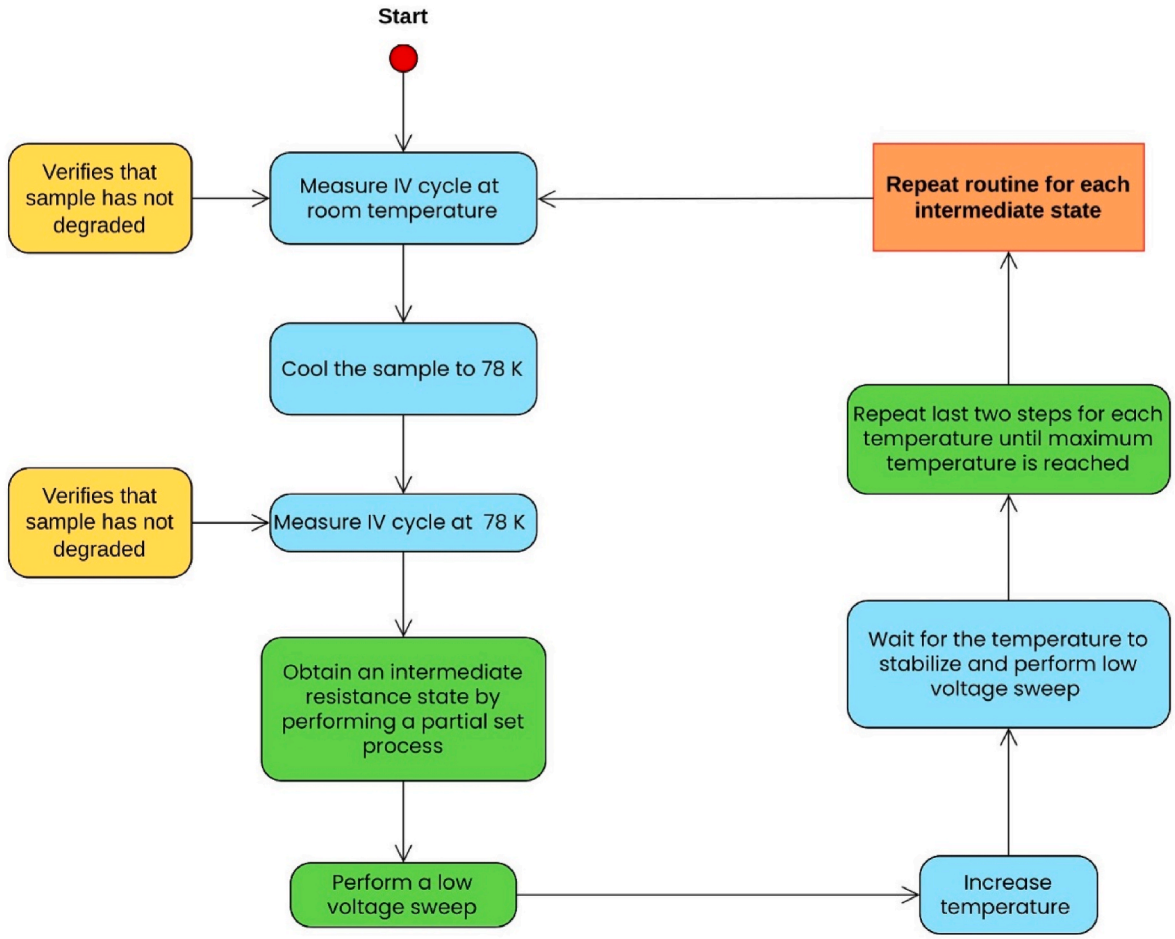

Fig. 3. Schematic of the experimental measurement routine process of the TiN/Ti/HfO_2/W devices.

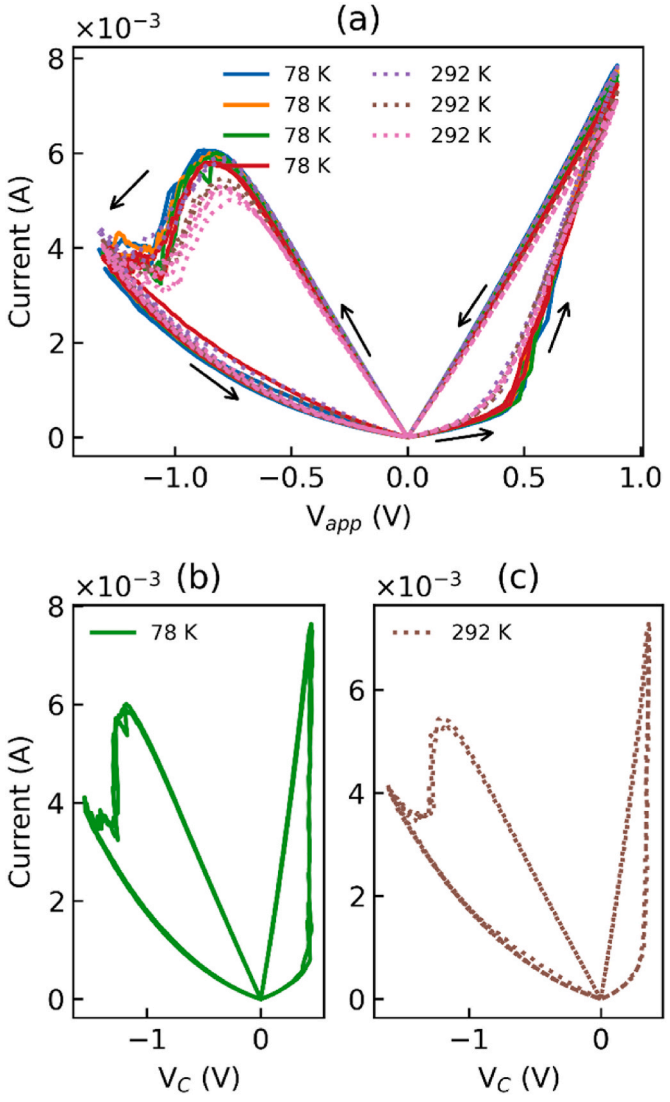

Fig. 4. (a) Measured I–V curves during resistive switching cycles performed at 78 K (solid lines) and 292 K (dashed lines). The devices show bipolar switching, with the reset process occurring at negative voltage and the set events at positive voltage (counter-clockwise RS). Modified I–V curves, which are calculated extracting the voltage drop in the series resistance [29,30] for the 78 K (b) and 292 K curves (c). Therefore, current in (b) and (c) is plotted versus the reduced voltage $V_C = V_{app} - I{\cdot}R_I$, where V_{app} is the applied voltage and R_I is the internal series resistance [29]: $R_I = 60\ \Omega$ (b) and $R_I = 74\ \Omega$ (c).

shows the modified I–V curves obtained after extracting the voltage drop in the series resistance, according to the methodology explained in Refs. [29,30]: the voltage in the switching region (V_C) (that is, the voltage that actually determines the switching processes) is the external applied voltage (V_{app}) minus the voltage drop in the series resistance (R_I):

$$V_C = V_{app} - I{\cdot}R_I \tag{1}$$

The resistance value is the one that generates the most vertical set transition in the modified plot I-V_C [29,30]. The following values have been obtained: $R_I = 60\ \Omega$ (RS performed at 78 K) and $R_I = 74\ \Omega$ (for the 292 K case).

With the aim of characterizing the thermal dependence of the current at different filament configurations, partial resistive switching cycles were performed with different maximum positive applied voltage (Fig. 5). In this way, the set process is limited and the CF (obtained after a set process until 0.9 V) is not completely rebuilt, but different partially formed CFs (with intermediate conductance values) are achieved. All

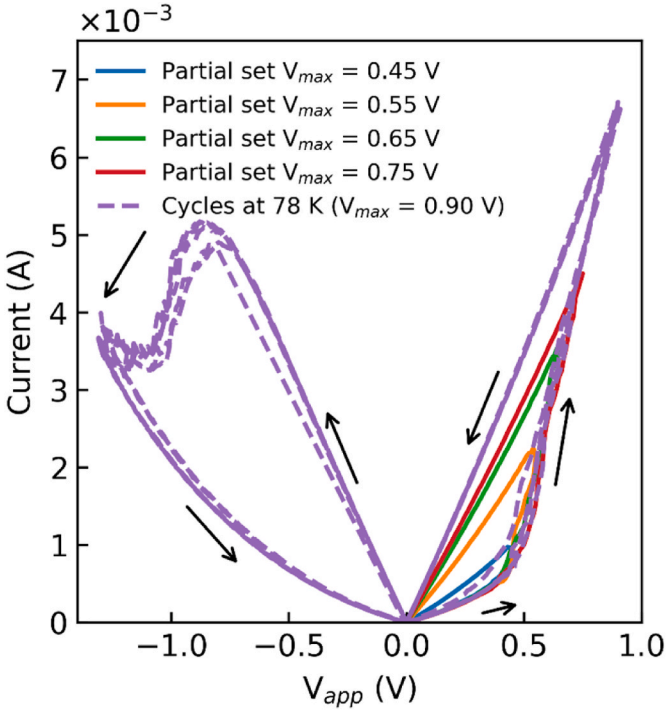

Fig. 5. Complete set-reset cycles performed at 78 K (purple dashed lines) and intermediate conductive states reached under the application of different maximum voltages (V_{max}) during the set process at 78 K.

these cycles were performed at 78 K. After the formation of each filament, the temperature is swept until 340 K. For each temperature, the I–V characteristics are obtained at low applied voltages (the maximum value is 0.15 V) in order to prevent changes in the filament configuration. In this way, all the variations in the measured current can be attributed to the thermal dependences of the charge transport mechanisms.

The current measured at different temperatures and conductive states is shown in Fig. 6. In the first column, the I–V plots are represented from the lowest conductive state (top, Fig. 6a) to the most conductive filament (bottom, Fig. 6m) for some selected temperatures for a better visualization. Note that the influence of the temperature is higher for the lowest conductive state. In order to better unravel the influence of the temperature on the current, second and third columns represent cross sections of plots in the first column (including the curves for all the temperatures): the current is plotted versus the temperature at fixed voltage in logarithmic (second column) and linear (third column) scales. The following dependences can be highlighted: i) the thermal dependence is smaller for lower temperatures than for higher temperatures; ii) the most conductive filament exhibits a metallic-like temperature dependence for the highest temperatures (approximately, higher than 190 K), while filaments formed by partial sets show an increase of the current when the temperature is increased; iii) For all the filaments, the current shows an elbow (an up-trend change in slope) at 270 K. The I–V curves were also measured at negative voltages (dashed lines in the first column of Fig. 6). As can be seen, a high degree of symmetry in the considered voltage range has been obtained.

4. Model description and discussion

The proposed model is a generalization of the previous development presented in Ref. [19] for the calculation of the conductance thermal dependence in the low resistive state (LRS) of TiN/Ti/HfO_2/Pt memristors. It is based on the widely used Stanford Model (SM) [31], although a series resistor is added (R_{CF}). This resistor is linked to the

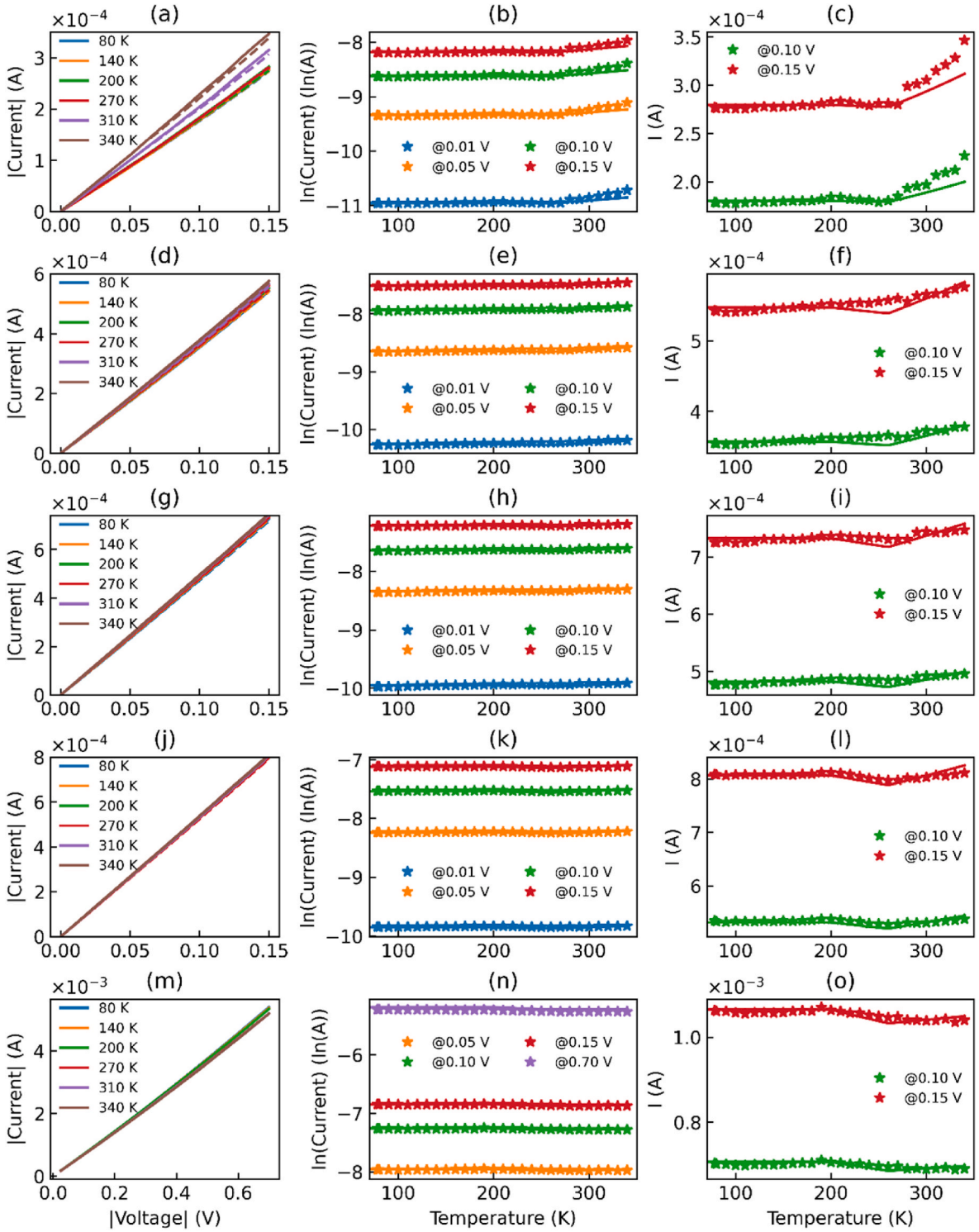

Fig. 6. Measured I–V curves in the devices programmed at several conductance states by means of using different stop voltages during the set voltage sweep: 0.45 V (a, b, c), 0.55 V (d, e, f), 0.65 V (g, h, i), 0.75 V (j, k, l) and 0.90 V (m, n, o). Once the device is programmed in a given state, the I–V characteristic was measured at different temperatures (a, d, g, j, m) at positive (solid lines) and negative (dashed lines) low voltages. Cuts of (a, d, g, j, m) curves at different voltages are plotted with star symbols in logarithmic scale in the current axis (figures b, e, h, k, n) and linear scale (figures c, f, I, l, o) in order to highlight the thermal dependences. In these latter sets of figures, the modeled curves obtained by simulation are plotted with solid lines.

conduction path to the switching region (wires, electrodes, fixed portion of the filament) [29] and it is necessary for modeling devices with a high degree of linearity in the low resistive states [19,26,30]. Its influence on the resistive switching behavior has been experimentally shown for the considered devices [30].

Therefore, as sketched in Fig. 7b, the model consists of an ohmic resistor (R_{CF}) and a non-linear behavioral current source, that depends on a state variable (g):

$$I_{NL}(g) = I_0 \cdot e^{-\frac{g}{g_0}} \cdot sinh\left(\frac{V}{V_0 - \beta\theta}\right) = I_0 \cdot e^{-\frac{g}{g_0}} \cdot sinh\left(\frac{V_{app} - I \cdot R_{CF}(T)}{V_0 - \beta\theta}\right) \quad (2)$$

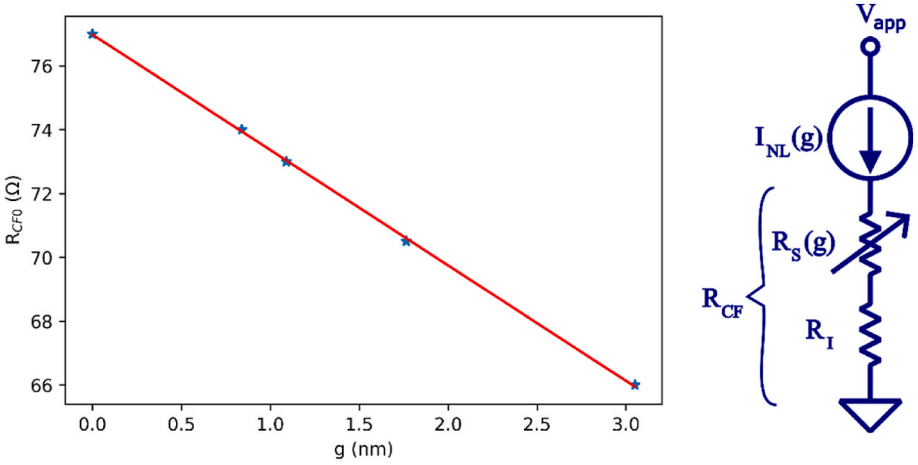

Fig. 7. (a) Symbols show the ohmic resistance (R_{CF}), at a reference temperature of 200 K (R_{CF0}), used for modeling the filaments at different conduction states, as a function of the model parameter *g* (gap distance between the filament tip and the electrode). The almost linear behavior allows a modelling approach based on a gap dependent variable resistance, as illustrated in panel (b).

where I_0, g_0 and V_0 are fitting parameters [31]. The state variable, *g*, is related to the distance between the filament tip and the electrode. Consequently, it is dependent on the programmed intermediate state. Note that equation (2) is the same than that of the SM, but including the voltage drop in the resistor R_{CF}. Furthermore, in order to reproduce the observed increment of the current as the temperature increases, a reduction of the parameter V_0 is applied, where β is a fitting parameter and $\theta = \max(0, T - T_b)$, being T_b also a fitting parameter, which corresponds to the temperature from which this equivalent barrier lowering is noted to start to influence. This methodology was previously employed in our former work [19]. A linear reduction of the barrier parameter with the temperature has also been used in other compact modeling approaches, as those based on the Quantum Point Contact model (QPC model) [20,24,32,33]. The origin of the non-linear transport component is not clearly established as it may be related to several mechanisms: the Schottky effect, tunnelling between the nearest traps and the electrode [18], trap-assisted tunnelling [26] or tunnelling through a barrier whose shape is modulated by the concentration of oxygen vacancies [15]. Therefore, the observed thermal dependence could be caused by a spreading of the electron energies, which could make more traps accessible, increase the direct tunneling transmission or improve capture/emission rates in trap-assisted tunneling processes, as recently proposed for Au/Ti/HfO_x/Au/devices [26]. In fact, several mechanisms could be involved, and more investigation is necessary for unveiling the origin of this measured thermal dependence. In this context, we used for modelling purposes an expression based on the SM, which is not linked to a specific transport mechanism, although it accounts for non-linear voltage and thermal dependences.

Note that, in expression (2), the voltage that actually determines the current of the non-linear component, I_{NL}, is calculated by subtraction of the voltage drop in the ohmic component, R_{CF}. The thermal dependence of this resistance is metallic-like and its calculated as follows:

$$R_{CF}(T) = \max\left(R_{CF0}, R_{CF0} \cdot [1 + \alpha \cdot (T - T_r)]\right) \quad (3)$$

Fig. 6 (second and third columns) shows the results obtained by the model (solid lines) and a comparison with the experimental current. A reasonable agreement has been achieved, despite the wide range of considered temperatures and the different trends observed in the filaments measured; in addition to the inherent device variability [13]. Table 1 shows the model parameters used, which are the same for all the filament states. Only the gap parameter, *g*, and the value of the ohmic resistance, R_{CF}, changes because the filament geometry is assumed to be different. Fig. 7 shows the relationship between the values of *g* and R_{CF0} used in the model for the five considered filament states.

Table 1
Model parameters.

Parameter	Value	Parameter	Value
I_0	3.03 mA	T_r	200 K
V_0	0.20 V	α	$9.5{\cdot}10^{-4}$ K^{-1}
β	$31{\cdot}10^{-5}$ V/K	T_b	260 K
g_0	1.5 nm		

In order to model the current at the different device intermediate states, and avoid using a different fitting parameter for each filament state (the value of R_{CF0}), the ohmic component is made dependent on the variable state, *g*, taking into account the relationship shown in Fig. 7a. With this purpose, R_{CF} is split off into two components (Fig. 7b): R_I and R_S. R_I is fixed (except for its thermal dependence, equation 3) and it is linked to the filament remnants that, basically, do not change during cycling (its length is assumed to be t_{ox} - g_{max}, being g_{max} the maximum allowed value for *g*, which corresponds to the HRS). On the other hand, R_S depends on the filament formation conditions (stop set voltage) through the variable state *g*. As far as *g* is interpreted as a gap distance between the filament tip and the electrode, and taking into account the linear dependence obtained in Fig. 7a, R_S can be calculated as follows:

$$R_S(g) = R_{Smax} \cdot \frac{(g_{max} - g)}{g_{max}} \quad (4)$$

where R_{Smax} is the resistance of the variable portion of the filament, when the filament is completely formed (LRS). With this approach, if the device state changes during a circuital simulation, the resistance is automatically recalculated and external re-tuning is not required.

Note that the minimum value of the ohmic resistance in Fig. 7a, that should be slightly higher than R_I (corresponding to $R_S \sim 0\ \Omega$, $g \sim g_{max}$), is coherent with the value of the serial resistance that has been independently calculated from the I–V curve in Fig. 4b.

In our previous work on TiN/Ti/HfO_2/Pt [19], the conductivity of the filament ohmic component showed a thermally activated behavior, with a low activation temperature. This dependence pointed out that the defects sub-band linked to the filament was very close to the Fermi level [15,34]. This behavior is not observed in the measured TiN/Ti/HfO_2/W devices, but the current shows almost a constant trend at the lowest temperatures, especially for the more conductive filaments, for which the ohmic component is expected to be more significant. Therefore, the energy of the filament sub-band is lower than the Fermi level [34]. Consequently, the thermal drift of the resistance given by equation (3) is the single thermal dependence considered for the ohmic resistance, R_{CF}.

The temperature from which this resistance increase starts to be noticeable, modeled by the parameter T_r, is similar in both types of devices.

Fig. 8 shows a comparison of the experimental conductance (blue surface) and the model results (red balls) as a function of the applied voltage and the temperature. The conductance is calculated as the measured current over the corresponding applied voltage. As can be seen, a good agreement has been achieved, taking into account that two input variables are swept and different filament configurations are considered with a single set of model parameters.

Once the model has been correctly tuned, it can be used for estimating the influence of the ohmic and non-linear components, their relative importance for the different intermediate states, and their values as a function of the temperature and the applied voltage. Fig. 9a shows the total resistance (solid lines), the ohmic resistance (R_{CF}, dotted lines) and the non-linear resistance (R_{NL}, dashed lines) for the partial filament rebuilt with a maximum set voltage of 0.45 V. Fig. 9b, c, 9d and 9e show the same resistances for the other device states, reached after the application of a maximum set voltage of 0.55 V, 0.65 V, 0.75 V and 0.90 V, respectively. Finally, Fig. 9f summarizes these results, showing the ratio R_{NL}/R_{CF} for all the considered filaments as a function of the temperature. As expected, R_{NL} is higher for the partially formed filaments, and the lower the set voltage, the higher its value. On the contrary, the influence of the ohmic component increases as the filament grows and it is the main component for the totally formed filament (Fig. 9e). For this reason, current increases as temperature rises in the partially formed filaments, while the contrary trend is observed for the most conductive filament at higher temperatures.

5. Conclusions

An experimental characterization of the current thermal dependence in TiN/Ti/HfO_2/W devices, programmed at different conductive states, has been carried out measuring the I–V characteristics at low voltages in order not to change the filament configuration. It is observed that the thermal dependence is weak at the lowest temperatures, while a significant change in the slope of the I–V curves is identified at 270 K. Conductive filaments formed at lower set voltages (partially formed filaments) show a current increase as the temperature rises (being the current change maximum for the less conductive state), while the fully formed filaments exhibit a metallic thermal dependence at higher temperatures.

A temperature dependent current model is proposed, based on the Stanford Model including an added series resistance. The model achieves good agreement with experimental data, taking into account that a wide range of temperatures for different filament configurations have been considered, showing diverse trends. The relative influence of ohmic and non-linear components in the different filament states is analyzed, showing that the non-linear component is more significant in partially formed filaments. In contrast, the ohmic component dominates in fully formed filaments.

Furthermore, the value of the series resistance can be easily calculated (from the modeled gap between the filament tip and the electrode) and it is coherent with that obtained independently from the experimental I–V cycles. In addition, the model is also consistent with the previously published model for the LRS in TiN/Ti/HfO_2/Pt devices.

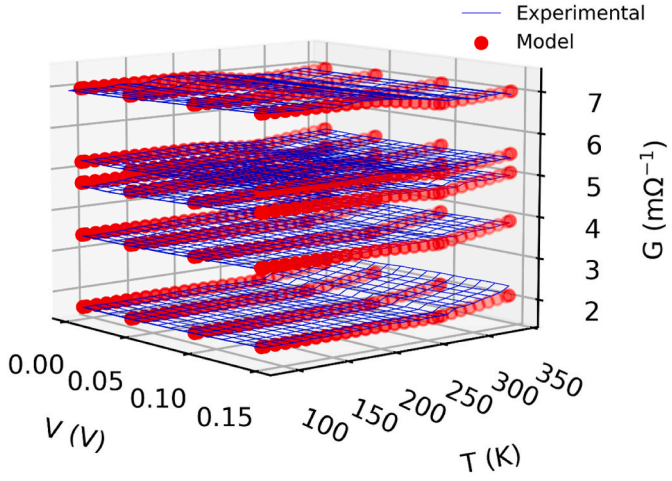

Fig. 8. Experimental (blue grid) and modeled (red balls) device conductance (calculated as V_{app}/I) versus the applied voltage and the temperature, for the different device conduction states.

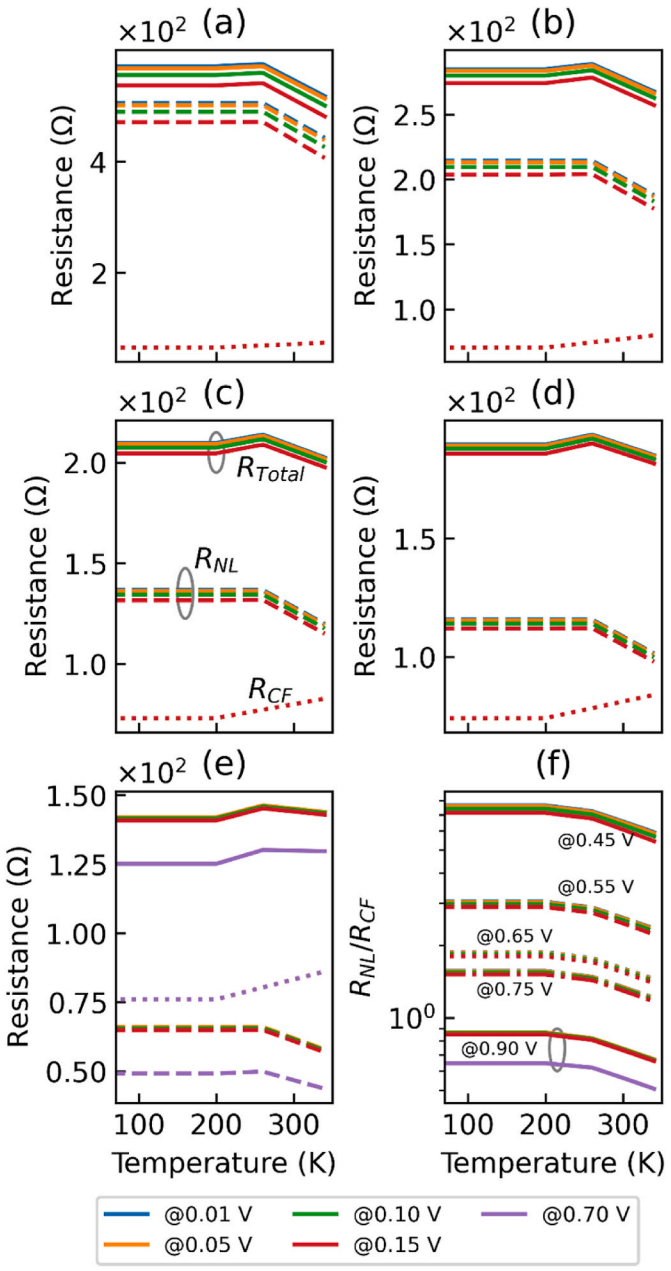

Fig. 9. Modeled total device resistance (solid lines) obtained by simulation with LT-spice (solid lines), for the several conductance states considered in this work using different set stop voltage: 0.45 V (a), 0.55 V (b), 0.65 V (c), 0.75 V (d) and 0.9 V (e). The line color indicates the read voltage. The contribution of the ohmic (R_{CF}) and non-linear (R_{NL}) components are also shown with dotted and dashed lines, respectively. Finally, figure (f) shows the R_{NL}/R_{CF} ratio for the data plotted in the former figures.

CRediT authorship contribution statement

F. Jiménez-Molinos: Writing – review & editing, Writing – original draft, Visualization, Methodology, Investigation, Funding acquisition, Formal analysis, Data curation, Conceptualization. **G. Vinuesa:** Writing – review & editing, Visualization, Methodology, Investigation, Formal analysis, Data curation, Conceptualization. **H. García:** Writing – review & editing, Visualization, Methodology, Investigation, Formal analysis, Data curation, Conceptualization. **S. Dueñas:** Writing – review & editing, Visualization, Resources, Methodology, Investigation, Funding acquisition, Formal analysis, Data curation, Conceptualization. **H. Castán:** Writing – review & editing, Visualization, Resources, Methodology, Investigation, Funding acquisition, Formal analysis, Data curation, Conceptualization. **M.B. González:** Writing – review & editing, Resources, Methodology, Investigation, Funding acquisition, Formal analysis, Conceptualization. **F. Campabadal:** Writing – review & editing, Resources, Methodology, Investigation, Funding acquisition, Formal analysis, Conceptualization. **J.B. Roldán:** Writing – review & editing, Visualization, Resources, Methodology, Investigation, Funding acquisition, Formal analysis, Data curation, Conceptualization.

Declaration of competing interest

The authors declare that they have no known competing financial interests or personal relationships that could have appeared to influence the work reported in this paper.

Data availability

Data will be made available on request.

Acknowledgements

We acknowledge grants PID2022-139586NB-C42, PID2022-139586NB-C43, PID2022-139586NB-C44 funded by MICIU/AEI/10.13039/501100011033 and FEDER, UE. IMB authors thank the CSIC funding through project 20225AT012 and the Generalitat de Catalunya-AGAUR for project 2021 SGR 00497. M.B.G. acknowledges the grant RYC2020-030150-I funded by MICIU/AEI/10.13039/501100011033 and by “ESF Investing in your future”.

References

[1] P. Jain, U. Arslan, M. Sekhar, B.C. Lin, L. Wei, T. Sahu, J. Alzate-vinasco, A. Vangapaty, M. Meterelliyoz, N. Strutt, A.B. Chen, P. Hentges, P.A. Quintero, C. Connor, O. Golonzka y Fis, 13.2 A 3.6Mb 10.1Mb/mm2 embedded non-volatile ReRAM macro in 22nm FinFET technology with adaptive forming/set/reset schemes yielding down to 0.5V with sensing time of 5ns at 0.7V, in: de 2019 IEEE International Solid- State Circuits Conference - (ISSCC), 2019.

[2] C.-C. Chou, Z.-J. Lin, C.-A. Lai, C.-I. Su, P.-L. Tseng, W.-C. Chen, W.-C. Tsai, W.-T. Chu, T.-C. Ong, H. Chuang, Y.-D. Chih, y T.-Y.J. Chang, A 22nm 96KX144 RRAM macro with a self-tracking reference and a low ripple charge pump to achieve a configurable read window and a wide operating voltage range, in: de 2020 IEEE Symposium on VLSI Circuits, 2020.

[3] W. Zhang, P. Yao, B. Gao, Q. Liu, D. Wu, Q. Zhang, Y. Li, Q. Qin, J. Li, Z. Zhu, Y. Cai, D. Wu, J. Tang, H. Qian, Y. Wang, H. Wu, Edge learning using a fully integrated neuro-inspired memristor chip, Science 381 (6663) (2023) 1205–1211.

[4] K. Zhu, S. Pazos, F. Aguirre, Y. Shen, Y. Yuan, W. Zheng, O. Alharbi, M. Villena, B. Fang, X. Li, A. Milozzi, M. Farronato, M. Muñoz-Rojo, T. Wang, R. Li, H. Fariborzi, J. Roldán, G. Benstetter, X. Zhang, H. Alshareef, T. Grasser, H. Wu, D. Ielmini y M. Lanza, Hybrid 2D–CMOS microchips for memristive applications, Nature 618 (2023) 57–62.

[5] R. Romero-Zaliz, E. Pérez, F. Jiménez-Molinos, C. Wenger, J.B. Roldán, Study of quantized hardware deep neural networks based on resistive switching devices, conventional versus convolutional approaches, Electronics 10 (3) (2021) 346.

[6] M. Akbari, S. Mirzakuchaki, D. Arumí, S. Manich, A. Gómez-Pau, F. Campabadal, M.B. González y R. Rodríguez-Montañés, True random number generator based on the variability of the high resistance state of RRAMs, IEEE Access 11 (2023) 66682–66693.

[7] H. Garcia, S. Dueñas, O.G.C.H. Ossorio, Current pulses to control the conductance in RRAM devices, IEEE Journal of the Electron Devices Society 8 (2020) 291–296.

[8] S. Poblador, M. Gonzalez, F. Campabadal, Investigation of the multilevel capability of TiN/Ti/HfO2/W resistive switching devices by sweep and pulse programming, Microelectron. Eng. 187–188 (2018) 148–153.

[9] R. Waser, D. Ielmini (Eds.), Resistive Switching. From Fundamentals of Nanoionic Redox Processes to Memristive Device Applications, Wiley-VCH, 2016.

[10] H. García, O.G. Ossorio, S. Dueñas, H. Castán, Controlling the intermediate conductance states in RRAM devices for synaptic applications, Microelectron. Eng. 215 (2019) 110984.

[11] V. Milo, C. Zambelli, P. Olivo, E. Pérez, M.K. Mahadevaiah, O.G. Ossorio, C. Wenger, D. Ielmini, Multilevel HfO2-based RRAM devices for low-power neuromorphic networks, Apl. Mater. 7 (8) (2019) 081120.

[12] P. Yao, H. Wu, B. Gao, J. Tang, Q. Zhang, W. Zhang, J.J. Yang y H. Qian, Fully hardware-implemented memristor convolutional neural network, Nature 577 (7792) (2020) 641–646.

[13] J.B. Roldán, E. Miranda, D. Maldonado, A.N. Mikhaylov, N.V. Agudov, A. A. Dubkov, M.N. Koryazhkina, M.B. González, M.A. Villena, S. Poblador, M. Saludes-Tapia, R. Picos, F. Jiménez-Molinos, S.G. Stavrinides, E. Salvador, F. J. Alonso, F. Campabadal, B. Spagnolo, M. Lanza, L.O. Chua, Variability in resistive memories, Advanced Intelligent Systems 5 (6) (2023) 2200338.

[14] R. Dittmann, S. Menzel, R. Waser, Nanoionic memristive phenomena in metal oxides: the valence change mechanism, Adv. Phys. 70 (2) (2022) 155–349.

[15] C. Funck, S. Menzel, Comprehensive model of electron conduction in oxide-based memristive devices, ACS Appl. Electron. Mater. 3 (2021) 3674–3692.

[16] S. Aldana, P. García-Fernández, R. Romero-Zaliz, M. González, F. Jiménez-Molinos, F. Gómez-Campos, F. Campabadal, J. Roldán, Resistive switching in HfO2 based valence change memories, a comprehensive 3D kinetic Monte Carlo approach, J. Phys. Appl. Phys. 53 (22) (2020) 225106.

[17] X. Chen, H. Li, Z. Tian, Y. Zhu, S. Longxing, Study of resistive switching behavior in HfO_2 nanocrystals synthesized via a low temperature hydrothermal method, Nanotechnology 35 (12) (2024) 125203.

[18] S. Yu, X. Guan y H.-S.P. Wong, «Conduction mechanism of TiN/HfOx/Pt resistive switching memory: a trap-assisted tunneling model, Appl. Phys. Lett. 99 (2011) 063507.

[19] F. Jiménez-Molinos, G. Vinuesa, H. García, A. Tarre, A. Tamm, K. Kalam, K. Kukli, S. Dueñas, H. Castán, M.B. González, F. Campabadal, J.B. Roldán, Thermal effects on TiN/Ti/HfO2/Pt memristors, J. Appl. Phys. 132 (2022) 194501.

[20] L.M. Prócel, L. Trojman, J. Moreno, F. Crupi, V. Maccaronio, R. Degraeve, L. Groux, E. Simoen, Experimental evidence of the quantum point contact theory in the conduction mechanism of bipolar HfO2-based resistive random access memories, J. Appl. Phys. 114 (2013) 074509.

[21] Y. Matveyev, K. Egorov, A. Markeev, A. Zenkevich, Resistive switching and synaptic properties of fully atomic layer deposition grown TiN/HfO2/TiN devices, J. Appl. Phys. 117 (4) (2015) 044901.

[22] C. Ahn, S. Kim, T. Gokmen, O. Dial, M. Ritter, H.-S.P. Wong, Temperature-dependent studies of the electrical properties and the conduction mechanism of HfOx-based RRAM, in: Proceedings of Technical Program - 2014 International Symposium on VLSI Technology, Systems and Application (VLSI-TSA), 2014.

[23] R. Fang, W. Chen, L. Gao, W. Yu, S. Yu, Low-temperature characteristics of HfOx-based resistive random access memory, IEEE Electron. Device Lett. 36 (6) (2015) 567–569.

[24] C. Walczyk, D. Walczyk, T. Schroeder, T. Bertaud, M. Sowinska, M. Lukosius, M. Fraschke, D. Wolansky, B. Tillack, E. Miranda y C. Wenger, «Impact of temperature on the resistive switching behavior of embedded HfO2-based RRAM devices, IEEE Trans. Electron. Dev. 58 (9) (2011) 3124–3131.

[25] V.A. Voronkovskii, V.S. Aliev, A.K. Gerasimova, D.R. Islamov, Conduction mechanisms of TaN/HfO x/Ni memristors, Mater. Res. Express 6 (7) (2019) 076411.

[26] F. Athena y E.M. Vogel, Describing the analog resistance change of HfOx-based neuromorphic synapses using a compact series trap-assisted tunneling and Ohmic conduction model, Appl. Phys. Lett. 123 (2023) 163506.

[27] A. Amirsoleimani, F. Alibart, V. Yon, J. Xu, M.R. Pazhouhandeh, S. Ecoffey, Y. Beilliard, R. Genov, D. Drouin, In-memory vector-matrix multiplication in monolithic complementary metal–oxide–semiconductor-memristor integrated circuits: design choices, challenges, and perspectives, Advanced Intelligent Systems 2 (11) (2020) 2000115.

[28] S. Yu, H. Jiang, S. Huang, X. Peng y A. Lu, Compute-in-Memory chips for deep learning: recent trends and prospects, IEEE Circ. Syst. Mag. 21 (3) (2021) 31–56.

[29] F.L. Aguirre, J. Suñé, E. Miranda, SPICE implementation of the dynamic memdiode model for bipolar resistive switching devices, Micromachines 13 (2) (2022) 330.

[30] D. Maldonado, F. Aguirre, G. González-Cordero, A.M. Roldán, M.B. González, F. Jiménez-Molinos, F. Campabadal, E. Miranda y J.B. Roldán, «Experimental study of the series resistance effect and its impact on the compact modeling of the conduction characteristics of HfO_2-based resistive switching memories, J. Appl. Phys. 130 (5) (2021) 054503.

[31] X. Guan, S. Wong, «A SPICE compact model of metal oxide resistive switching memory with variations, IEEE Electron. Device Lett. 33 (10) (2012) 1405–1407.

[32] A. Avellán, E. Miranda, D. Schroeder, Model for the voltage and temperature dependence of the soft breakdown current in ultrathin gate oxides, J. Appl. Phys. 97 (2005) 014104.

[33] M. Calixto, D. Maldonado, E. Miranda, J. Roldán, Modeling of the temperature effects in filamentary-type resistive switching memories using quantum point-contact theory, J. Phys. Appl. Phys. 53 (2020) 295106.

[34] D. Ielmini, F. Nardi, C. Cagli, Physical models of size-dependent nanofilament formation and rupture in NiO resistive switching memories, Nanotechnology 22 (2011) 254022.